Journal of Colloid and Interface Science 445 (2015) 277–284

Contents lists available at ScienceDirect

Journal of Colloid and Interface Science

www.elsevier.com/locate/jcis

Covalent immobilization of molecularly imprinted polymer nanoparticles using an epoxy silane

Tripta Kamra [a,b,c], Shilpi Chaudhary [a,b,c], Changgang Xu [b], Niclas Johansson [a], Lars Montelius [c,d], Joachim Schnadt [a,*], Lei Ye [b,*]

[a] Division of Synchrotron Radiation Research, Department of Physics, Lund University, Box 118, 22100 Lund, Sweden
[b] Division of Pure & Applied Biochemistry, Lund University, Box 124, 22100 Lund, Sweden
[c] ENI AB, Malmö, Sweden
[d] Division of Solid State Physics, Department of Physics, Lund University, Box 118, 22100 Lund, Sweden

GRAPHICAL ABSTRACT

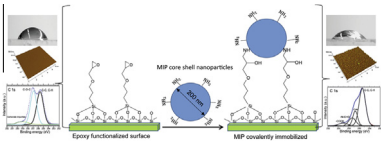

ARTICLE INFO

Article history:
Received 16 October 2014
Accepted 25 December 2014
Available online 7 January 2015

Keywords:
Molecularly imprinted polymers
Epoxy silane
Self-assembled monolayer
X-ray photoelectron spectroscopy
Propranolol
Molecular recognition

ABSTRACT

Molecularly imprinted polymers (MIPs) can be used as antibody mimics to develop robust chemical sensors. One challenging problem in using MIPs for sensor development is the lack of reliable conjugation chemistry that allows MIPs to be fixed on transducer surface. In this work, we study the use of epoxy silane to immobilize MIP nanoparticles on model transducer surfaces without impairing the function of the immobilized nanoparticles. The MIP nanoparticles with a core–shell structure have selective molecular binding sites in the core and multiple amino groups in the shell. The model transducer surface is functionalized with a self-assembled monolayer of epoxy silane, which reacts with the core–shell MIP particles to enable straightforward immobilization. The whole process is characterized by studying the treated surfaces after each preparation step using atomic force microscopy, scanning electron microscopy, fluorescence microscopy, contact angle measurements and X-ray photoelectron spectroscopy. The microscopy results show that the MIP particles are immobilized uniformly on surface. The photoelectron spectroscopy results further confirm the action of each functionalization step. The molecular selectivity of the MIP-functionalized surface is verified by radioligand binding analysis. The particle immobilization approach described here has a general applicability for constructing selective chemical sensors in different formats.

1. Introduction

Many biological macromolecules (e.g. antibodies, proteins, enzymes, and aptamers) exhibit a highly fine-tuned and effective molecular recognition ability, which makes them suitable for chemical and biological sensors [1–3]. However, typically these natural receptors are costly and have problems with stability (chemical and physical) and sensitivity in non-optimal

Abbreviations: MIPs, molecularly imprinted polymers; SAM, self-assembled monolayer; GPTMS, (3-glycidoxypropyl)trimethoxysilane; XPS, X-ray photoelectron spectroscopy; AFM, atomic force microscope; SEM, scanning electron microscope.

* Corresponding authors.
E-mail addresses: joachim.schnadt@sljus.lu.se (J. Schnadt), lei.ye@tbiokem.lth.se (L. Ye).

http://dx.doi.org/10.1016/j.jcis.2014.12.086
0021-9797/

environments [4] and therefore it is often necessary to switch to synthetic receptors with high stability and cost effectiveness. A new recent development is the use of molecularly imprinted polymers (MIPs) with predesigned molecular selectivity produced by template driven polymerization [5,6]. The MIPs can be fabricated directly *in situ* on a transducer surface to act as a molecular recognition layer for detection of the template or its structural analogs. For example, imprinted polymer films for detection of heparin have been fabricated on an electrode in a potentiometric sensor [7]. A micro patterned thin MIP film imprinted with testosterone has also been reported in a holographic sensor [8]. A major problem associated with the *in situ* fabricated MIP sensors is, however, the inaccessibility of a large fraction of template sites due to the layers' small surface area. With *ex situ*-prepared MIP-based sensors the problem can be circumvented since these MIPs can be synthesized as particles with a large surface-to-volume ratio. In the approach the MIPs are prepared *ex situ* using emulsion [9] or precipitation polymerization [10] and then attached to the transducer surface either directly or through a polymer layer, as reported by Reimhult et al. for QCM-D sensors [11] and Kröger et al. for an electrochemical sensor [12]. A drawback of using polymer layer-based conjugation chemistry is the thickness of the interface layer, which can affect the MIP particles' sensitivity. Here we are looking for an approach that is designed not to affect the sensitivity of the sensing material, which is achieved by minimizing the contact between the transducer and MIP surfaces. At the same time the contact is stable and allows the formation of a smooth and uniform MIP particle layer. The contact layer consisting of highly oriented epoxy silane linker molecules is formed via a self-assembled monolayer (SAM). The structurally oriented SAM can be prepared easily with high reproducibility [13].

The SAMs of organosilanes have proved to be useful for functionalization of different silica surfaces like quartz, silicon wafers and glass. The MIP particles can be immobilized electrostatically or covalently using SAM modified surfaces. As an example, recently an optical MIP sensor was fabricated by Kolarov et al. using a SAM of 3-aminopropyltriethoxysilane (APTES), where the positively charged amine allowed attachment of the negatively charged MIP particles [14]. However, electrostatic attachment does not offer sufficient particle fixation, particularly in the presence of electrolytes or in highly basic/acidic solutions. Therefore, it is necessary to develop suitable methods for the covalent immobilization of MIP particles. Recently, we used perfluorophenylazide-mediated photoconjugation chemistry [15–17] to immobilize MIP particles [18]. The azide groups are activated by UV light and the generated nitrenes undergo CH insertion reactions leading to a covalent immobilization of the MIP particles. This approach results in a dense coverage of MIP particles, but the morphology is rough and difficult to control and thus not desirable for sensing applications [19]. Here we instead report another approach for covalent immobilization, with which smooth and uniform layers of MIP particles immobilized on a surface can be achieved (*cf.* Scheme 1). We used propranolol-imprinted MIP nanoparticles and immobilize them directly on GPTMS functionalized glass. The uniform and stable silane functionalized glass surface has epoxide terminal groups, which are available to covalently attach amine functionalized MIP core–shell nanoparticles via an epoxide ring opening reaction [20]. The covalently immobilized MIP particles are in close contact with the surface due to short length of the epoxy silane linker (<2 nm) and retain their binding sites for the template (propranolol) as shown by a radioligand binding analysis. The surfaces are characterized by scanning electron microscopy (SEM), atomic force microscopy (AFM), fluorescence microscopy, measurement of the water contact angle and X-ray photoelectron spectroscopy (XPS). The approach for immobilizing MIP particles described here is straightforward and does not require special photoactive chemicals. It is applicable for conjugation of core–shell MIP particles on epoxy-functionalized surfaces in different sensor constructs.

2. Materials and methods

2.1. Materials

Acetone, acetic acid (glacial, 100%), acetonitrile (99.7%), azobisisobutyronitrile (AIBN, 98%) were purchased from Merck (Darmstadt, Germany). Methacrylic acid (MAA, 98.5%) was purchased from ACROS (Geel, Belgium). Propranolol hydrochloride (99%) supplied by Fluka (Dorset, UK) was converted into free base form before use. Allylamine (98%). *N*-isopropylacrylamide (NIPAM) and *N*,*N*-methylene-bis-acrylamide (MBA) were purchased from Monomer–Polymer Laboratories (Windham, USA) and ICN Biomedicals Inc. (Warrendale, USA), toluene, (3-glycidoxypropyl)trimethoxysilane (GPTMS, 98%), pindolol (free base) from Sigma–Aldrich, propranolol, L-[4-^{3}H] (specific activity 20 curie/mmol, 50 μM) from NEN Life Science Products (Boston, MA, USA), and 1-amino-3-(naphthalen-1-yloxy) propan-2-ol (free base) from Aurora Feinchemie GmbH (Graz, Austria). Before use, AIBN was re-crystallized from methanol. All other chemicals were used as received. Microscopic glass slides were purchased from Menzel (Germany). A Kodak storage phosphor screen TR (^{3}H) sensitive imaging plate (20×25 cm^{2}) was purchased from CardiRad (Sweden). A 1-inch n-doped Si wafer with phosphorous as dopant material was used to prepare samples for XPS analysis and template binding measurements. The resistivity of the wafer was 1–10 Ω cm^{-1}, *i.e.* the dopant concentration varied from 4×10^{15} cm^{-3} to 5×10^{14} cm^{-3}.

2.2. Methods

To study the roughness and homogeneity of the prepared surfaces tapping-mode AFM was carried out in ambient environment using an instrument by Veeco (New York, USA). The n-doped silicon cantilever tip with a typical curvature radius of 10 nm, a force constant ≈10–130 N/m (PPP-NCHR-20), a spring constant of 10–130 N/m and a resonance frequency of 204–497 kHz was obtained from Veeco (Plainview, New York, USA). The AFM images were analyzed using the Nanoscope software by Digital Instruments. Additional SEM characterization was carried out using a SEM LEO 1560 (Zeiss, Oberkochen, Germany) operated at 10 kV. To avoid charging the samples were coated with a 10 nm Pt coating prior to SEM imaging.

Initial probing of the immobilized MIP particles on GPTMS-functionalized glass surfaces were achieved using fluorescence microscopy with a Nikon Eclipse E-400 microscope (excitation wavelength 495 nm, probed emission wavelength 525 nm) equipped with a CCD camera (Andor Technology, Belfast, Northern Ireland). Prior to the measurements a fluorescein isothiocyanate (FITC) dye was attached to the sample surfaces by dipping them for 16 h at room temperature into a 0.1 mg/mL solution. Before imaging the samples were washed in acetonitrile to remove any excess dye. As a control experiment the same procedure was applied to piranha solution-treated blank slides. Static contact angle measurements were performed using a Contact Angle Module CA-1 from Sinterface Technologies (Berlin, Germany). A 5 μl drop of Millipore water was dropped on the surface and the images were recorded after a few seconds of contact.

XPS was performed at the spectroscopy end station of beamline I311 at the MAX IV Laboratory in Lund, Sweden [21]. The instrument with separate preparation and analysis chambers (base pressures better than 10^{-10} mbar) and a sample load lock is equipped with a Scienta SES 200 hemispherical electron energy analyzer. The samples were prepared *ex situ* and mounted on the sample

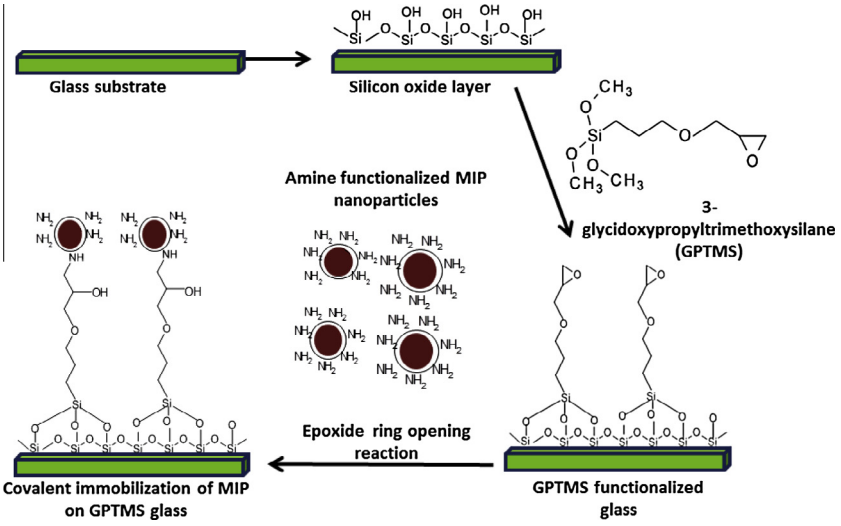

Scheme 1. Process of immobilization of core–shell MIP nanoparticles using a SAM of GPTMS as binding layer.

holder using double-sided adhesive carbon tape. To avoid sample charging expected for non-conducting samples the glass slides were replaced by a n-doped Si (100) wafer. Good electrical contact of the surface with ground was ensured by establishing a direct contact between the sample surface and sample holder using conductive carbon tape. The measurements were started after introduction of the sample and subsequent degassing once the pressure had recovered to 10^{-8} mbar. The X-ray photoelectron (XP) spectra were recorded in normal (emission angle 0° from the surface normal) and grazing (75°) emission geometries. All spectra were calibrated by reference to the Si 2p peak for silicon dioxide peak at 103.2 eV binding energy [22]. Shirley or polynomial backgrounds were removed from all spectra.

Radioligand binding analysis was performed to study the molecular selectivity of the MIP-coated surfaces. For these experiments a two inch silicon wafer (specifications same as above) was cut into pieces of 10×10 mm^2 size. The pieces were then functionalized with GPTMS and incubated in MIP particle and non-imprinted polymer (NIP) suspensions for 16–18 h at room temperature. The resulting surfaces were washed in 20% acetic acid solution in methanol twice and then in acetonitrile to remove any pyridine left after particle immobilization. The surfaces were then incubated for 12 h at room temperature with ^{3}H-labeled propranolol solution in acetonitrile (100 nM), after which they were rinsed in acetonitrile and left for a few minutes to dry. Finally, the surfaces were left for 18 h at room temperature in a cassette that ensured intimate contact between the sample surfaces and the tritium-sensitive screen. The tritium-sensitive screen was then analyzed using a FUJIFILM Fluorescent Image Analyzer FLA 3000 with a laser wavelength of 635 nm. The image analyzer generated signal patterns from the photographic film, which converts β particles from the radioactive decay into photostimulable luminescence [23]. In this way the luminescence intensity is in proportion to the quantity of the radioligand bound on the sample surface. Further data analysis was carried out using the Origin Pro 9.1 software.

2.3. Synthesis of the MIP nanoparticles

Molecularly imprinted core–shell nanoparticles were synthesized in two steps according to the procedure reported by Hajizadeh et al. [24]. In the first step, (*R*,*S*)-propranolol (137 mg, 0.53 mmol) was dissolved in 40 mL of acetonitrile in a (150×25 mm) borosilicate glass tube equipped with a screw cap. MAA (113 mg, 1.31 mmol), TRIM (648 mg, 2.02 mmol) and AIBN (28 mg) were then added to the solution. The solution was purged with a gentle flow of nitrogen for 5 min and then sealed. Polymerization was carried out in a Stovall HO-10 Hybridization Oven at 60 °C (Greensboro, NC, USA), in which the sample was rotated at a speed of 20 rpm for 24 h. The polymerization step led to the formation of propranolol imprinted core particles. In the second step, NIPAM (566 mg, 5 mmol), MBA (77.2 mg, 0.5 mmol), allylamine (188 μL, 2.5 mmol), and AIBN (24 mg) were added into the reaction tube and sonicated for 3 min. The mixture was then purged with nitrogen for 5 min before the mixture was allowed to polymerize for 48 h under a gentle rotation in an oven at 60 °C. After the second polymerization the reaction mixture was centrifuged at 11,300 g for 15 min to collect the polymer particles. The template was removed by washing the core–shell particles with methanol containing 10% acetic acid (v/v), until no template could be detected from the washing solvent by UV spectrometry using a wavelength of 290 nm. The polymer particles were finally washed with acetone and dried in a vacuum chamber. The core–shell NIP particles were synthesized using the same protocol as described above, but without the template in the pre-polymerization mixture.

2.4. Preparation of silanized glass

The glass slides were cut into pieces of 10×10 mm^2 size, which were cleaned in 2 M NaOH solution for a few minutes. The slides were then rinsed using distilled water and kept in 0.5 M HCl for 2 h, after which they were washed thoroughly under distilled water. The cleaned glass surfaces were activated in piranha solution (H_2O_2:H_2SO_4, 7:3 v/v) for 45 min at 75 °C to generate the Si–OH groups (*cf.* Scheme 1). After activation the glass slides were washed thoroughly in distilled water, blown dry in N_2 gas and kept in an oven for a few minutes to rid the surface of water. The activated glass slides were then immersed for 16 h in GPTMS (2%, v/v) in an anhydrous toluene solution at 50 °C [25]. After that the silanized surfaces were rinsed thoroughly in toluene and then sonicated in toluene for a few seconds to remove any agglomerated silane present on glass. Finally, the glass surfaces were dried under N_2 and kept in an oven at 100 °C for 24 h.

2.5. Immobilization of the MIP nanoparticles

The MIP nanoparticles were suspended in pyridine:water (1:1, v/v) solution (3 mg/mL) and sonicated for about 10–15 min. After

silanization, the GPTMS functionalized glass slides, together with a piranha solution-treated blank slide were immersed for 12 h in a MIP suspension (*cf.* Scheme 1). After that the slides (GPTMS and blank) were washed thoroughly in pyridine:water (1:1, v/v) solution for a few minutes and finally sonicated for a few seconds to remove all the physiosorbed MIP nanoparticles from the surface. For radioligand binding experiments, the surfaces were neutralized in 20% acetic acid in methanol, followed by washing in acetonitrile. Finally, the slides were dried under N_2 and stored in vacuum until characterization.

3. Results and discussion

Scheme 1 illustrates the approach used for immobilization of the MIP nanoparticles. In this approach, the surface was first hydroxylated and then functionalized with GPTMS. In the final step the surface was exposed to a solution of core–shell MIP particles (or core–shell NIP particles as a reference) to finish the nucleophilic substitution reaction. The density of the epoxy groups was tailored to achieve a high availability of epoxy groups for MIP particle attachment, while ensuring the uniformity of the silane layer. The ideal concentration of GPTMS was found to be 2%, at which both homogeneity and high density of epoxides on the glass surface were achieved (see Electronic Supplementary Material, Fig. S1).

Table 1 provides a short description of the surfaces prepared according to the scheme, which then were characterized by different methods. Table also specifies the terminology for the remainder of the text. The "glass", "G-Epoxy" and "G-Epoxy-MIP" preparations represent the single steps in Scheme 1. For benchmarking we also studied surfaces for which certain steps of the preparation had been eliminated. The "G-Epoxy-MIP∗" preparation represents the entire process of Scheme 1, but with the final sonication omitted, thus allowing assessment of the aggregation of physisorbed MIP particles. For the "G-MIP" surface the GPTMS functionalization was omitted, while for the "G-Epoxy-NIP" surface the entire preparation process was performed, but with NIP rather than with MIP nanoparticles. For the XPS measurements and radio ligand binding studies we replaced glass with a silicon wafer. The Si wafer surfaces were prepared in the same way as the microscopy glass slide in Scheme 1 and are represented as Si, Si-Epoxy, Si-Epoxy-MIP and Si-Epoxy-NIP (*cf.* Table 1).

3.1. Self-assembled monolayer of epoxy silane

After cleaning, the first step of preparation is the treatment of the surface with GPTMS with the goal of achieving a SAM. Fig. S2 shows the change in the water droplet angle as we move from glass (Fig. S2A) to epoxy silane (Fig. S2B). The contact angle of <5° for the glass increases to 55° for the G-Epoxy surface, which is in line with what has been observed previously [26]. The observation clearly

Table 1
Short description of studied surfaces.

Surface	Description	
Glass	Piranha cleaned glass	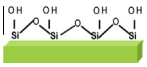
G-Epoxy	Epoxy functionalized microscopic glass	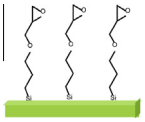
G-Epoxy-MIP∗	Immobilized MIP on glass before sonication	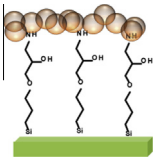
G-Epoxy-MIP	Immobilized MIP on glass after sonication	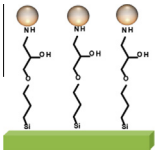
G-MIP	Glass with physisorbed MIP after sonication	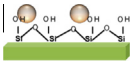
Si	Piranha cleaned silicon wafer	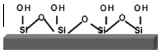
Si-Epoxy	Epoxy functionalized silicon wafer	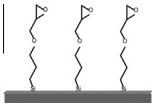
Si-Epoxy-MIP	Immobilized MIP on silicon wafer after sonication	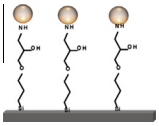
Si-Epoxy-NIP	Immobilized NIP on silicon wafer after sonication	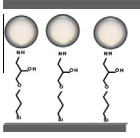

indicates that the piranha solution-treated glass surface is clean and hydrophilic as expected for a hydroxylated surface, while the G-Epoxy surface is more hydrophobic as a result of the GPTMS treatment.

AFM reveals a smooth and uniform G-Epoxy sample (RMS roughness of 3 nm) with few islands (Fig. 1A). The images are quite similar to what is observed using SEM (Fig. S3B). Also the SEM images of the glass shows a homogenous and smooth surface morphology (Fig. S3A).

The XP spectra provide additional insight about the elemental information of the surfaces. The overview spectrum obtained on the Si-Epoxy surface in Fig. 2A shows a strong increase in C 1s and N 1s intensity upon GPTMS treatment in comparison to the spectra measured on the Si surface, for which only a small carbon contamination peak is seen. Also the Si 2s, Si 2p and O 1s lines change significantly. This confirms the functionalization of the Si slides – treated in the same way as the glass slides – with GPTMS (*cf.* Table 1).

The C 1s XP spectra measured in grazing and normal emission geometries are normalized to the maximum height of the signal and are shown together in Fig. 2B, where their components can be compared. Three components are found, the first of which at 285.20 eV, we assign to photoemission from the carbon atoms bonded to carbon, hydrogen and silicon (denoted C—C, C—H). The second component at 286.89 eV is due to photoemission from oxygen-bonded carbon atoms and thus comprises the signal from the epoxy group [27]. Finally, at highest binding energy we find a peak that we suggest is due to carbonate impurities due to the possible reaction of the epoxide groups on the surface with atmospheric carbon dioxide at high temperature in the oven [28,29]. When measured in grazing emission, the intensity ratio between the two main components changes in comparison to the spectrum measured in normal emission geometry: the peak intensity ratio of the two main components is almost 1, whereas it decreases in the grazing emission spectrum. This is a clear indication of that the epoxide groups are available on the surface with high density.

3.2. MIP immobilization

Fig. 3 shows the fluorescence images obtained on the G-MIP, G-Epoxy-MIP∗, and G-Epoxy-MIP surfaces. The FITC dye, with which the samples were treated before imaging, contains an isothiocyanate group reactive toward the amino, but not the epoxy groups. No fluorescence is observed for the G-MIP surface (Fig. 3A). A strong, inhomogeneous fluorescence signal is seen for the G-Epoxy-MIP∗ sample (Fig. 3B), whereas a somewhat weaker but rather homogeneous signal is found for the G-MIP surface (for more quantitative information see figure caption in Fig. 3). Hence, no MIP particle attachment occurs on the G-MIP surface, while the G-Epoxy-MIP∗ sample is characterized by significant MIP particle aggregation. Clearly, sonication leads to removal of physisorbed excess MIP particles as seen in the case of the G-Epoxy-MIP sample (Fig. 3C).

The water contact angle decreases from 55° to 20° between the G-Epoxy and G-Epoxy-MIP surfaces, *i.e.* after MIP immobilization (Fig. S2). This implies that the surface becomes hydrophilic in line with our expectations: the MIP core shell nanoparticles are hydrophilic due to the presence of the abundant amino groups in the shell. The AFM image of the G-Epoxy-MIP sample in Fig. 1C shows a dense packing of the MIP particles on the surface compared to the control, G-MIP in Fig. 1A. From the AFM sectional view (Fig. S4) we find that the G-Epoxy-MIP sample is significantly rougher (with RMS roughness of 45 nm) than the G-MIP sample (RMS roughness of 2 nm), indicating that MIP particles are immobilized on the G-Epoxy-MIP sample, but not on the G-MIP sample. We can also observe the similar homogeneity and particle coverage between G-Epoxy-MIP and Si-Epoxy-MIP (Fig. 1C and D). Hence, the presence of epoxy groups on the G-Epoxy surface is of crucial

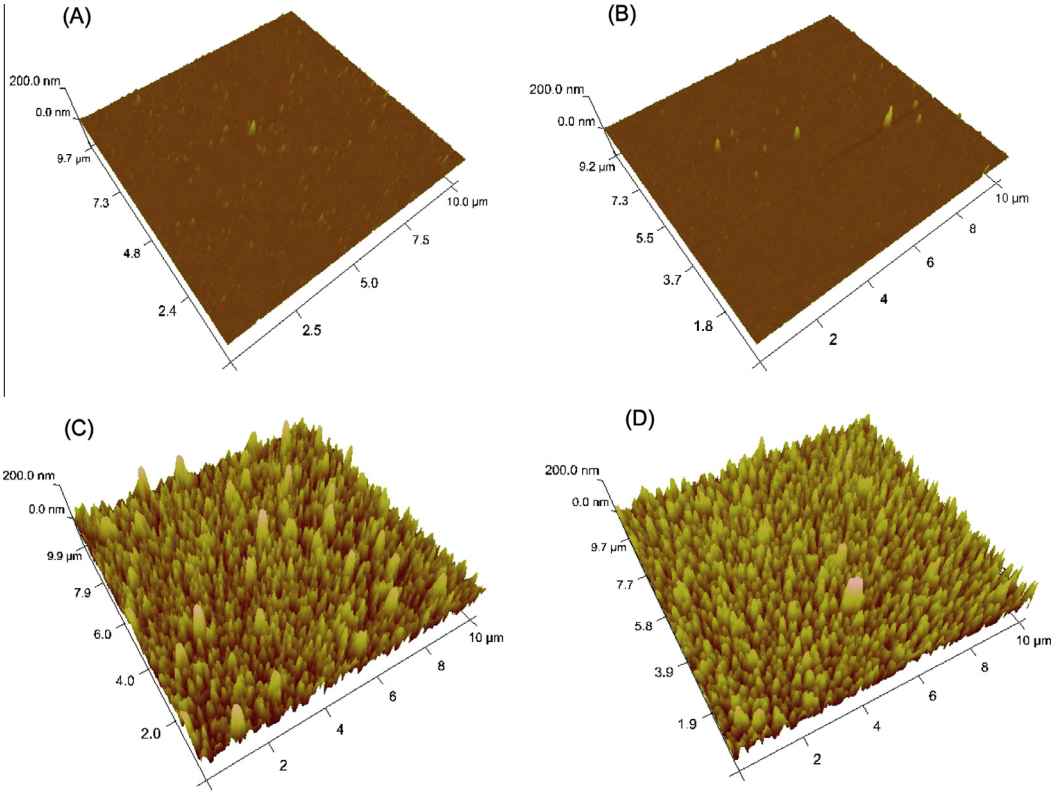

Fig. 1. Tapping mode 3D AFM topographical images for the different surfaces studied: (A) G-MIP, (B) G-Epoxy, (C) G-Epoxy-MIP and (D) Si-Epoxy-MIP.

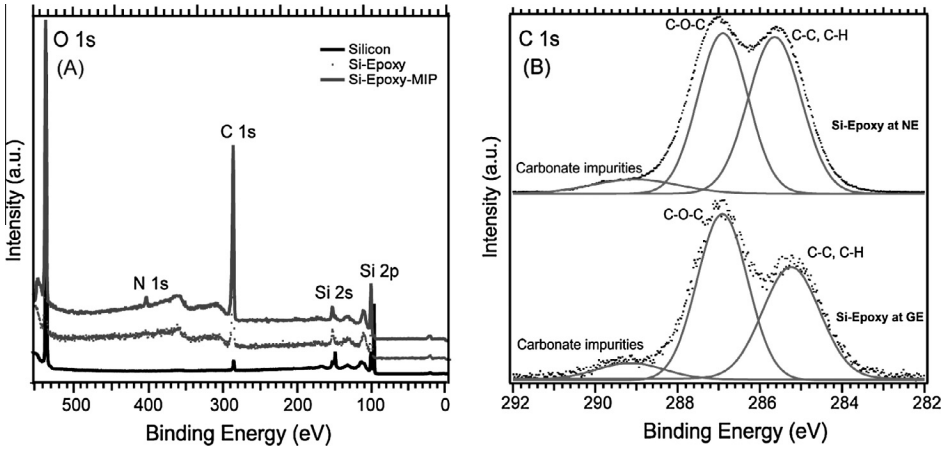

Fig. 2. (A) Overview XP spectrum: the N 1s peak at 401.1 eV is a fingerprint of the MIP core shell nanoparticles. (B) Comparison of C 1s spectra of Si-Epoxy measured in normal emission (NE, more bulk sensitive) and grazing emission (GE, more surface sensitive) geometries.

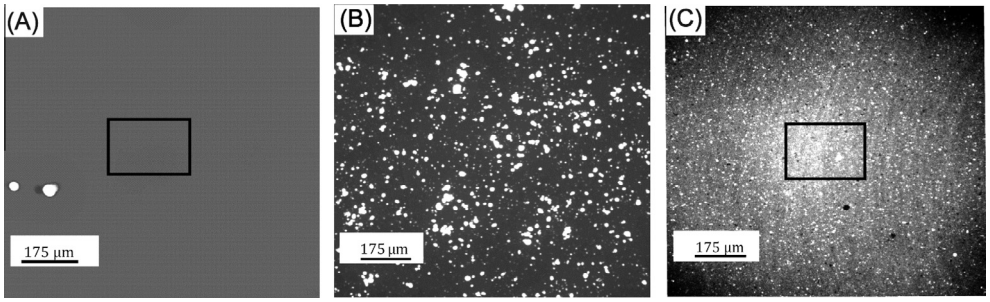

Fig. 3. Fluorescence microscopy measurements: (A) G-MIP surface, no fluorescence, (B) G-Epoxy-MIP* surface, and (C) G-Epoxy-MIP surface. The number of photocounts in the marked region is 39 in (A) and 30,000 in (C).

importance for the immobilization of the MIP particles. From the SEM image of G-Epoxy-MIP (Fig. S3D), the average number of MIP particles immobilized on a $10 \times 10\ mm^2$ area was estimated to be 6×10^{10}.

The XPS overview in Fig. 2A confirms the successful immobilization of MIP particles on the Si-Epoxy-MIP surface: the N 1s peak at around 400.1 eV binding energy is due to the amino groups of the MIP particles, and further the C 1s peak at around 285 eV is significantly enhanced in comparison to the Si and Si-Epoxy surface due to the immobilized organic polymer particles.

Fig. 4A and B shows the C 1s and N 1s XP spectra measured on the Si-Epoxy-MIP surface. C 1s components are found at 285.10, 286.68, 287.89 and 289.20 eV binding energy, which we attribute to aliphatic (C—C/C—H), nitrogen-bonded (C—N), nitrogen- and oxygen-bonded (N—C=O), and carboxyl carbon (—COOH), respectively [30,31]. The N 1s line shows features at 400.23, 402.52 and 407.00 eV binding energy due to the free amine [32] of the MIP particles, cationic ammonium groups [33] and possible nitrates [34] that are derived from oxidation of the organic amines in the MIP nanoparticles. The presence of these components is as expected for the XP spectra of the MIP particles. Fig. 4C shows the O 1s line for the Si-Epoxy and Si-Epoxy-MIP samples. The O 1s line of the Si-Epoxy-MIP is significantly broader than that of the Si-Epoxy surface, in particular when measured in grazing emission. We attribute this to the presence of a carbonyl oxygen (O=C) at ~534.50 eV binding energy [35] in line with the structure of the MIP nanoparticles, which contain carbonyl groups derived from the NIPAM and MBA monomer. In normal emission geometry the O 1s line appears somewhat narrower which indicates that the carbonyl groups are found primarily on the surface of the MIP particles. Overall, we find clear evidence for MIP immobilization on the GPTMS treated surfaces, which we attribute to a nucleophilic epoxide ring opening reaction between the core–shell particles and the surface bonded epoxide groups.

3.3. Verification of molecular recognition surfaces

To apply MIP-modified surfaces for chemical sensing, it is critical that the molecular selectivity of the immobilized MIP particles is not sacrificed during the conjugation reaction. In this work we used autoradiography technique to verify that the chemical conjugation to the GPTMS modified surface does not affect the interior binding sites of the core–shell MIP particles.

Fig. 5 shows the images obtained in the radioligand binding analysis. For the Si sample (Fig. 5A) no contrast is seen, which implies that no radioactive template binding has taken place. For the Si-Epoxy-MIP sample (Fig. 5B) a large contrast and thus saturation of the surface with the template is observed. Also for the Si-Epoxy-NIP surface, the image signal is weak and only slightly higher than that observed from the Si surface. The photoluminescence intensity of each image is calculated using Origin Pro 9 and the values are depicted as integrated signal intensity (a.u.) after background subtraction against sample area (Fig. S5A).

The image intensity from the Si-Epoxy-MIP sample is 8 times of that from the Si sample and 4 times from the Si-Epoxy-NIP sample, which indicates clearly that the MIP particles retain their high template affinity after the chemical immobilization.

To prove more clearly the molecular selectivity of Si-Epoxy-MIP, we performed competitive radioligand binding experiment on this surface by adding excess competitive compounds to the

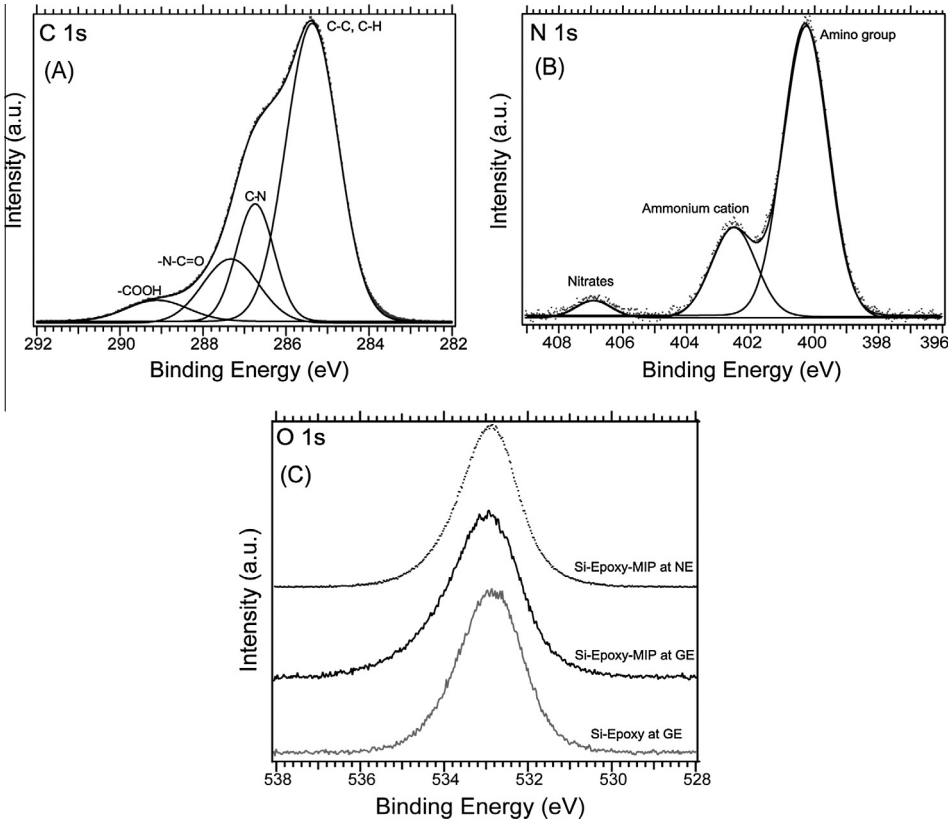

Fig. 4. XP spectra: (A) C 1s and (B) N 1s spectrum of the Si-Epoxy-MIP sample (normal emission geometry), (C) O 1s spectrum of the Si-Epoxy sample measured at a grazing emission angle together with the spectra of the Si-Epoxy-MIP sample in both normal and grazing emission geometries.

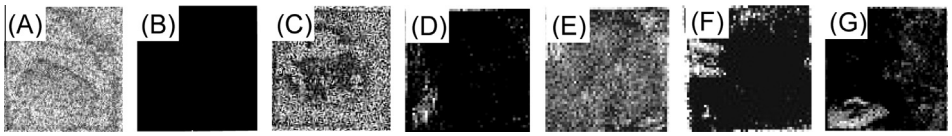

Fig. 5. Autoradiography images showing the ^{3}H labeled propranolol binding to three different surfaces: (A) Si, (B) Si-Epoxy-MIP, (C) Si-Epoxy-NIP. Autoradiography images showing ^{3}H labeled propranolol binding to Si-Epoxy-MIP in the absence of competing compound (D), and in the presence of 10 μM propranolol (E), pindolol (F), and ANOP (G).

labeled propranolol solution. The three competitive compounds used are unlabeled propranolol, pindolol and 1-amino-3-(naphthalen-1-yloxy) propan-2-ol (ANOP) (*cf.* Fig. 6). In principle, addition of the competing compounds into the radioligand binding solution should displace the labeled propranolol from the surface, and the degree of displacement should be determined by the molecular similarity of the competing compound to the labeled template. As can be seen from Fig. 5D–G, the binding of the labeled propranolol to the Si-Epoxy-MIP decreased the most, by 48%, when unlabeled propranolol was added as the competitive compound. Pindolol, a structural analog of propranolol, only decreased the radioligand binding by 20%. The other competing compound, ANOP did not show any displacement effect due to the lack of the terminal isopropyl group. Collectively, the Si-Epoxy-MIP surface displays clear molecular selectivity, which can only be attributed to the intact molecular binding sites located in the immobilized MIP particles.

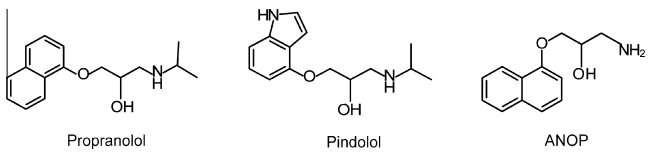

Fig. 6. Structure of the template molecule (propranolol) and its analoges (pindolol and ANOP).

4. Conclusions

We have developed an approach to immobilize core–shell MIP nanoparticles on epoxy SAMs. Our data suggest strongly that the bond of the MIP particles to the surface has a covalent character and it seems feasible to assume that an epoxy ring opening reaction is responsible for this strong MIP attachment. An important feature of this method is its versatility for the homogeneous and covalent immobilization of even materials with a relatively large size. The chemistry does not involve any interfacial polymer layer which helps in direct molecular sensing applications [36]. Moreover, the coupling reaction is easy, reproducible, and efficient without affecting the specificity and molecular recognition properties of the MIP nanoparticles toward the template. Thus the method is applicable to various amine functionalized materials for lab-on-chip and other sensing applications [37,38]. The approach does not require high temperature, photo- or chemical activation, which renders the method physically and chemically more robust and handy in comparison to other immobilization procedures.

Acknowledgments

We are grateful for financial support by the European Commission via the Marie Curie Initial Training Network SMALL (grant no. 238804) as well as by Vetenskapsrådet (grant no. 2010-5080). Further we would like to thank Per-Olof Larsson for helping with the Fluorescence microscope measurements, Tommy Nylander for access to the instrument for contact angle measurements, and Sofi Elmorth and Alak Alshiekh for helping with the autoradiography imaging.

Appendix A. Supplementary material

Water contact angle measurements, SEM images, AFM cross section profiles, intensity profiles of autoradiography images.

Supplementary data associated with this article can be found, in the online version, at http://dx.doi.org/10.1016/j.jcis.2014.12.086.

References

[1] J. Wang, Electroanalysis 13 (2001) 983–988.
[2] J.J. Gooding, Electroanalysis 14 (2002) 1149–1156.
[3] M. Liss, B. Petersen, H. Wolf, E. Prohaska, Anal. Chem. 74 (2002) 4488–4495.
[4] V.J.B. Ruigrok, M. Levisson, M.H.M. Eppink, H. Smidt, J. van der Oost, Biochem. J. 436 (2011) 1–13.
[5] X. Ding, P.A. Heiden, Macromol. Mater. Eng. 299 (2014) 268–282.
[6] K. Haupt, K. Mosbach, Chem. Rev. 100 (2000) 2495–2504.
[7] L. Li, Y. Liang, Y. Liu, Anal. Biochem. 434 (2013) 242–246.
[8] Y. Fuchs, O. Soppera, A.G. Mayes, K. Haupt, Adv. Mater. 25 (2013) 566–570.
[9] N.P. Moral, A.G. Mayes, Langmuir 20 (2004) 3775–3779.
[10] K. Yoshimatsu, K. Reimhult, A. Krozer, K. Mosbach, K. Sode, L. Ye, Anal. Chim. Acta 584 (2007) 112–121.
[11] K. Reimhult, K. Yoshimatsu, K. Risveden, S. Chen, L. Ye, A. Krozer, Biosens. Bioelectron. 23 (2008) 1908–1914.
[12] S. Kröger, A.P.F. Turner, K. Mosbach, K. Haupt, Anal. Chem. 71 (1999) 3698–3702.
[13] N.K. Chaki, K. Vijayamohanan, Biosens. Bioelectrons. 17 (2002) 1–12.
[14] F. Kolarov, K. Niedergall, M. Bach, G. Tovar, G. Gauglitz, Anal. Bioanal. Chem. 402 (2012) 3245–3252.
[15] L.H. Liu, M. Yan, Acc. Chem. Res. 43 (2010) 1434–1443.
[16] J.F.W. Keana, S.X. Cai, J. Org. Chem. 55 (1990) 3640–3647.
[17] T. Kubo, X. Wang, Q. Tong, M. Yan, Langmuir 27 (2011) 9372–9378.
[18] S. Chaudhary, T. Kamra, K.M.A. Uddin, O. Snezhkova, H.S.N. Jayawardena, M. Yan, L. Montelius, J. Schnadt, L. Ye, Appl. Surf. Sci. 300 (2014) 22–28.
[19] Y. Kuriu, A. Kawamura, T. Uragami, T. Miyata, Chem. Lett. 43 (2014) 825–827.
[20] T. Dubrovsky, A. Tronin, S. Dubrovskaya, S. Vakula, C. Nicolini, Sens. Actuat. B 23 (1995) 1–7.
[21] R. Nyholm, J.N. Andersen, U. Johansson, B.N. Jensen, I. Lindau, Nucl. Instrum. Methods Phys. Res., Sect. A 467–468 (2001) 520–524.
[22] H. Kobayashi, Y. Yamashita, K. Namba, Y. Todokoro, Appl. Surf. Sci. 108 (1997) 433–438.
[23] A.M. Kellerer, J. Chen, H. Roos, Radiat. Environ. Biophys. 32 (1993) 183–191.
[24] S. Hajizadeh, C. Xu, H. Kirsebom, L. Ye, B. Mattiasson, J. Chromatogr. A 1274 (2013) 6–12.
[25] V. Tsukruk, I. Luzinov, D. Julthongpiput, Langmuir 15 (1999) 3029–3032.
[26] M.S. Islam, H. Yu, H.G. Lee, S.H. Kang, Biosens. Bioelectron. 26 (2010) 1028–1035.
[27] S.J. Sofia, V. Premnath, E.W. Merrill, Macromolecules 31 (1998) 5059–5070.
[28] F. Shi, Q. Zhang, Y. Ma, Y. He, Y. Deng, J. Am. Chem. Soc. 127 (2005) 4182–4183.
[29] R.P. Vasquez, J. Electron Spectrosc. Relat. Phenom. 56 (1991) 217–240.
[30] L.H. Liu, G. Zorn, D.G. Castner, R. Solanki, M.M. Lerner, M. Yan, J. Mater. Chem. 20 (2010) 5041–5046.
[31] J. Ji, L. Li, K. Xia, L. Li, S. Shang, J. Macromol. Sci. Part A Pure Appl. Chem. 49 (2012) 316–320.
[32] M.T. Lee, G.S. Ferguson, Langmuir 17 (2001) 762–767.
[33] T. Meylheuc, C. Methivier, M. Renault, J.M. Herry, C.M. Pradier, M.N.B. Fontaine, Colloids Surf. B 52 (2006) 128–137.
[34] C. Nanayakkara, P. Jayaweera, G. Rubasinghege, J. Baltrusaitis, V. Grassian, J. Phys. Chem. A 118 (2014) 158–166.
[35] Y.P. Wang, K. Yuan, Q.L. Li, L.P. Wang, S.J. Gu, X.W. Pei, Mater. Lett. 59 (2005) 1736–1740.
[36] A. Kulkarni, Y. Xu, C. Ahn, R. Amin, S.H. Park, T. Kim, M. Lee, J. Biotechnol. 160 (2012) 91–96.
[37] C.F. Wan, C.S. Chen, K.C. Hwang, Y.H. Laid, J.Y. Luo, P.C. Liu, L.S. Fan, Sens. Actuat. B 193 (2014) 53–61.
[38] Y. Han, A. Offenhausser, S. Ingebrandt, Surf. Interface Anal. 38 (2006) 176–181.